DTU Library

Spectral tensor parameters for wind turbine load modeling from forested and agricultural landscapes

Chougule, Abhijit S.; Mann, Jakob; Segalini, A.; Dellwik, Ebba

[Link back to DTU Orbit](#)

RESEARCH ARTICLE

Spectral tensor parameters for wind turbine load modeling from forested and agricultural landscapes

A. Chougule[1], J. Mann[1], A. Segalini[2] and E. Dellwik[1]

[1] DTU Wind Energy, Risø Campus, Frederiksborgvej 399, 4000 Roskilde, Denmark
[2] KTH Mechanics, Osquars Backe 18, SE-100 44 Stockholm, Sweden

ABSTRACT

A velocity spectral tensor model was evaluated from the single-point measurements of wind speed. The model contains three parameters representing the dissipation rate of specific turbulent kinetic energy, a turbulence length scale and the turbulence anisotropy. Sonic anemometer measurements taken over a forested and an agricultural landscape were used to calculate the model parameters for neutral, slightly stable and slightly unstable atmospheric conditions for a selected wind speed interval. The dissipation rate above the forest was nine times that at the agricultural site. No significant differences were observed in the turbulence length scales between the forested and agricultural areas. Only a small difference was observed in the turbulence anisotropy at the two sites, except near the surface, where the forest turbulence was more isotropic. The turbulence anisotropy remained more or less constant with height at the forest site, whereas the turbulence became more isotropic with height for the agricultural site. Using the three parameters as inputs, we quantified the performance of the model in coherence predictions for vertical separations. The model coherence of all the three velocity components was overestimated for the analyzed stability classes at both sites. As expected from the model approximations, the model performed better at both sites for neutral stability than slightly stable and unstable conditions. The model prediction of coherence of the along-wind and vertical components was better than that of the cross-wind component. No significant difference was found between the performance of the model at the forested and the agricultural areas. © 2014 The Authors. Wind Energy published by John Wiley & Sons, Ltd.

1. INTRODUCTION

An adequate description of the structure of atmospheric turbulence is important for the calculation of dynamic loads on wind turbines. The classical concepts used for describing such structure include the velocity spectra, co-spectra and the cross-spectral properties coherence and phase.[1–3] Spectral analysis is useful for analysis of the length scales inherent in turbulent motion.[4] In addition to the length scale estimations, coherences are also important to wind engineers.[5] Coherences are usually described as a function of separation normal to the mean wind direction.[6]

Spectral tensor models are often used to model the spectra and cross-spectra,[7] and such models can be used for the estimation of dynamic loads on turbines through simulation of the wind field toward the rotor. Models developed by Kaimal *et al.*,[8] Veers (Sandia method),[9] and Mann[10] are commonly used in wind-energy industry. The three-dimensional spectral tensor model of Mann (M94) differs from the other models mentioned earlier in many respects. It incorporates rapid distortion theory (RDT)[3,11] with an assumption of uniform mean shear and consideration of eddy life time, while the model by Kristensen *et al.*[7] is a kinematic model, and the models by Kaimal *et al.*[8] and Veers[9] are more empirical models incorporating many model parameters. The stationary M94 model assumes homogeneity of the neutral surface-layer

turbulence. RDT has previously been used in non-stationary spectral tensor modeling of homogeneous uniform sheared,[12] unsheared stably stratified,[13] and sheared stably stratified[14] turbulent flows.

The International Electrotechnical Commission (IEC)[15] recommends the use of M94 for the estimation of loads on wind turbines through simulation of rotor inflow.[16] The spectral shapes and coherences that the model predicts have previously been compared with the data measured over sea, over a flat rural terrain and even in boundary-layer wind tunnels.[17] In these studies, coherences of the along-wind, cross-wind and vertical velocity components (*u*, *v* and *w*, respectively) have been found to decrease with increasing cross-wind separation distance, which matched with both observation and theoretical predictions,[10] but coherences of all the velocity components for given vertical separations have never been estimated. The boundary-layer wind-tunnel testing described by Mann[17] showed that the wind tunnel turbulence was slightly more isotropic than the natural turbulent wind. None of the M94 tests were conducted beyond 70 m above the terrain. Later, the model one-point spectra were fitted to observations of wind speed made by sonic anemometer at higher heights even for non-neutral conditions, although the model was not extended to account for the effects of thermal stratification.[18] The study conducted by Peña *et al.*[18,19] demonstrated a close connection between the mixing length derived from the wind speed profile and the turbulence length scale from the M94 model. The spectral tensor resulting from the fitting of the measured one-point spectra was used to investigate how dynamic wind loads depend on atmospheric stability.[20] However, the cross-spectral properties were never investigated in the studies described in the literature.[18–20] The exception from only looking at one-point spectra was the study by Chougule *et al.*,[21] who compared the predicted two-point cross-spectral phases (which provide the arrival time shift of turbulence at two heights) with measurements. Chougule *et al.*[21] demonstrated that the *v*-phase φ_v was significantly greater than the *u*-phase φ_u, which in turn was greater than the *w*-phase φ_w for $k_1 \Delta z \leq 1$, where k_1 is the stream-wise wavenumber and Δz is the vertical separation, and the M94 model predicted this phase behavior correctly. The Sandia method,[9] on the other hand, assumes an average of zero phase between any two points such that the imaginary parts of the cross-spectra are zero. However, the actual consequence of the differences in the cross-spectral phases on the wind loads of horizontal axis wind turbines has never been studied.

Generally, wind turbines are placed in open landscapes with low aerodynamic roughness; hence, wind engineering model tools have been developed keeping in mind that they have to perform well in such conditions. However, during the last decade, the siting of wind turbines in forested areas has become increasingly common. One of the drawbacks associated with forested areas is the increased load on the rotor caused by the high turbulence levels of the atmospheric flow. The present model has never been compared with turbulence spectra measured over a forest, let alone the comparison with two-point statistics such as coherences or cross-spectral phases. It is therefore highly relevant to extend the validation to data taken in forested areas.

In this study, we investigated the performance of the M94 model concerning the prediction of velocity spectra measured over a forest, compared the parameters describing the model spectra with those from a low-roughness agricultural landscape and tested the performance of the model in coherence predictions for both the agricultural and forested sites. This study differs from the previous studies mainly in the following respects:

1. Validation of M94 in a forested area
2. Evaluation of coherences of all three velocity components for vertical separation
3. Quantification of the model performance in the prediction of coherences

Our approach to the study is described in Section 2. For the analysis, we used data from two different sites, the Ryningsnäs site in Sweden (forested landscapes) and the Høvsøre test site in Denmark (agricultural landscapes), as described in Section 2.1. We selected the data based on the selection criteria described in Section 2.2, followed by the spectral tensor modeling described in Section 2.3. Analyses of both observed and modeling results are provided in Section 3, with discussions in more detail in Section 4. We conclude our study in Section 5 with some final considerations and guidelines.

2. METHOD

We estimated the velocity spectra and co-spectrum of *u* and *w* from the measured time series as

$$F_{ij}(f,z) \equiv \langle \hat{u}_i(f)\hat{u}_j^*(f) \rangle, \tag{1}$$

where $i,j = 1, 2, 3$; $(u_1, u_2, u_3) = (u, v, w)$; f is the frequency; $\langle \rangle$ denotes ensemble average operator; the superscript $*$ denotes complex conjugate and $\hat{u}_i(f)$ is the complex-valued Fourier transform of the *i*th velocity component at height *z*.

We selected the data according to the classification of atmospheric stability in terms of the Obukhov length L_o following Gryning *et al.*,[22] where L_o is defined as[1]

$$L_o = \frac{-u_*^3}{\kappa(g/T)\overline{w'T'}_0}, \tag{2}$$

where u_* is the surface friction velocity, $\kappa = 0.4$ is the von Kármán constant, g is the acceleration due to gravity, T is the mean surface-layer temperature and $\overline{w'T_0'}$ is the vertical kinematic heat flux density at the surface. The measured spectra and co-spectra given in equation (1) change with atmospheric stability;[8] i.e., $F_{ij}(f, z)$ is a function of L_o.

We performed χ^2-fits[10] of the M94 model to the measured power spectra in equation (1) to obtain the three parameters (described in Section 2.3) that were used as inputs to estimate the model cross-spectra. The basic idea of the χ^2-fit was to minimize the sum of the squared differences between the theoretical and the estimated u-spectra, v-spectra, w- spectra and uw co-spectra. Model coherences and cross-spectral phases were compared with those from the measurements. The cross-spectra, coherences and cross-spectral phases were calculated from the measurements using general definitions, which can be found in the study of Chougule *et al.*[21]

2.1. Experimental data

Experimental data were obtained from the measurements taken at two different sites: the forested landscapes in Ryningsnäs (where data were taken from a mast above the forest canopy) and a sector with flat agricultural terrain at the Høvsøre test site in Denmark. Wind speed measurements were taken with Metek sonic anemometers (USA-1, Metek Gmbh, Elmshorn, Germany) with a sampling frequency of $f = 20$ Hz and measuring in three dimensions. The measurement data were block averaged after applying corrections for flow distortion[23] and cross-wind correction.[24] Statistical analyses were based on 30-min intervals.

2.1.1. Ryningsnäs.

The 138-m tall tower at Ryningsnäs is located in a relatively flat, forested terrain in Southeastern Sweden at $57°16.57'$N, $15°59.19'$E. Data from the sector between $235°$ and $275°$ were selected. In this sector, the influence from a local clearing as well as two nearby turbines to the south and the north-east, respectively, is avoided. Further, the flow distortion from the mast on the measurements is minimal, and the upstream terrain is forested for more than 100 km, such that the whole boundary layer should be adapted to the high surface roughness. The forest near the tower is 20–25 m tall and consists mainly of Norway spruce (*Pinus sylvestris*). Generally, the forest cover is not homogeneous but rather consists of patches of different tree heights intercepted with clearings, lakes and lower-roughness areas.

The sonic anemometers were installed at the heights of 40, 59, 80, 98, 120 and 138 m. The measurements were performed between November 2010 and February 2012. More information on the site and the measurements can be found in the study of Bergström *et al.*[25]

2.1.2. Høvsøre.

The measurements were taken from the 116.5-m tall mast located at the coordinates $56°26'26''$N, $08°09'03''$E in the Høvsøre test site near the west coast of Denmark. Sonic anemometers were installed on the mast at heights of 10, 20, 40, 60, 80 and 100 m. The land to the east of the mast is flat, consisting mostly of agricultural landscapes. Five wind turbines were placed to the north of the mast. To avoid the wake effects of wind turbines, winds were selected from the region between $60°$ and $120°$. Around $65°$ and at 8 km from the mast, there are lines of trees and a big forest that extends about 12 km in both north–south and east–west directions. A small village is situated at approximately $100°$ about 2.8 km from the mast, which could also have affected the flow downstream to west. On the west side of the mast, land extends 1500 m to the North Sea coast, including a dune. More details about the location and instrumentation can be found in the literature.[20, 26] The analysis was carried out using 7 years of data from 2004 to 2010.

2.2. Data selection

Data from both the sites were selected based on a narrow wind speed interval measured at 80 m height as well as bins of L_o measured at 40 and 10 m on the masts at Ryningsnäs and Høvsøre sites, respectively. Because of limitations on the availability of data and in order to compare the results from two sites, we analyzed near-neutral stable (NNS), neutral (N), and near-neutral unstable (NNU) stability cases (the stability classes are defined in Table I). Since the results for the other wind speeds were similar, the results for the wind speed bin 7–8 ms^{-1} only are provided.

Table I. Classification of atmospheric stability according to the Obukhov length intervals (in m^{-1}).

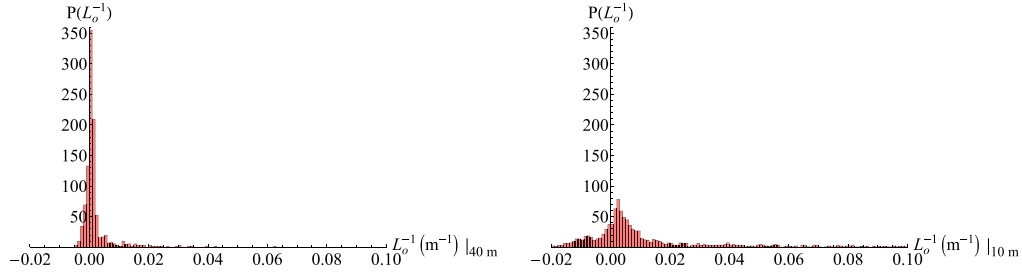|	
Near-neutral stable (NNS)	$0.002 \leq L_o^{-1} \leq 0.005$
Neutral (N)	$|L_o^{-1}| \leq 0.002$
Near-neutral unstable (NNU)	$-0.005 \leq L_o^{-1} \leq -0.002$

Figure 1. Histogram of atmospheric stabilities based on the Obukhov lengths for wind directions between 235° and 275° at the Ryningsnäs test site in Sweden (left graph) and for wind directions between 60° and 120° at the Høvsøre test site in the west coast of Denmark (right graph), for the velocity bin 7–8 ms^{-1}.

Figure 1 shows the histogram of atmospheric stability in terms of L_o from the Ryningsnäs (left graph) and Høvsøre (right graph) sites, for the velocity bin 7–8 ms^{-1}. For this wind speed interval, hardly any occurrences of very stable or very unstable cases were observed at the Ryningsnäs site, and the histogram at Ryningsnäs was generally narrower. Both observations were caused by the higher roughness at Ryningsnäs and consequently a stronger mechanically generated turbulence.

2.3. Spectral tensor model

The velocity-spectrum tensor $\Phi_{ij}(\boldsymbol{k})$ contains the information about the second-order statistics of all the three velocity components through indices i, j, where $\boldsymbol{k}$ is a three-dimensional wavenumber vector. Also, by definition, $\Phi_{ij}(\boldsymbol{k})$ represents the Reynolds-stress 'density' in wavenumber space.[11] The modeled $\Phi_{ij}(\boldsymbol{k})$ of M94 is valid in the neutral surface-layer with the assumption of uniform shear dU/dz. Depending upon their orientation in the plane of uniform shear, the eddies will stretch or compress via $\boldsymbol{k}(t) = (k_1, k_2, k_{30} - k_1(dU/dz)t)$, where t is time (to visualize the motion, see Pope[11]/Chapter 11/Figure 11.5 c on page 407).

The model calculates the evolution of Fourier modes $\hat{u}_i(\boldsymbol{k})$ (i.e., three-dimensional Fourier transform of the velocity components for $i = 1, 2$ and 3) under the influence of the mean shear from an initial isotropic state, and $\Phi_{ij}(\boldsymbol{k})$ was modeled through,

$$\frac{\langle \hat{u}_i^*(\boldsymbol{k}) \hat{u}_j(\boldsymbol{k}) \rangle}{dk_1 dk_2 dk_3} = \Phi_{ij}(\boldsymbol{k}). \tag{3}$$

The equation for the evolution of the Fourier modes was deduced from the linearized Navier–Stokes equations via RDT, where the time-dependent, random nature of the turbulent field in physical space implies the time dependence and randomness of the field $\hat{u}_i(\boldsymbol{k})$ (in Fourier space).

In isotropic turbulence, the velocity-spectrum tensor is

$$\Phi_{ij}(\boldsymbol{k}_0) = \frac{E(k)}{4\pi k^2} \left(\delta_{ij} - \frac{k_i k_j}{k^2} \right), \tag{4}$$

where $\boldsymbol{k}_0 = \boldsymbol{k}(0)$ and k is the length of the vector $\boldsymbol{k}$. The energy spectrum $E(k)$ given by von Kármán[27] as

$$E(k) = \alpha \epsilon^{2/3} L^{5/3} \frac{(kL)^4}{(1 + (kL)^2)^{17/6}}, \tag{5}$$

where $\alpha \approx 1.7$ is the spectral Kolmogorov constant, ϵ is the rate of viscous dissipation of specific turbulent kinetic energy (TKE) and L is a turbulence length scale.

The stretching of eddies due to shear for an infinitely long time is unrealistic, since the eddies must break at some point because of the stretching. The small-scale more isotropic turbulent eddies are not affected by shear. In order to make the spectral tensor stationary, the time dependency in the model was removed by incorporating the general concept of an eddy life time, $\tau(k)$. In the inertial sub-range, the life time of eddies is proportional to $k^{-2/3}$, and the assumption in the M94 model was, at scales, larger than the inertial sub-range; eddy life time is proportional to k^{-1} divided by their characteristic velocity $\left(\int_k^\infty E(p) dp \right)^{1/2}$ such that $\tau(k)$ is proportional to $k^{-2/3}$ for $k \to \infty$ and k^{-1} for $k \to 0$, where E was chosen as equation (5). The parameterization of $\tau(k)$ in M94 was

$$\tau(k) = \Gamma \left(\frac{\mathrm{d}U}{\mathrm{d}z}\right)^{-1} (kL)^{-2/3} \left[{}_2F_1\left(\frac{1}{3}, \frac{17}{6}; \frac{4}{3}; -(kL)^{-2}\right)\right]^{-1/2}, \tag{6}$$

where Γ is a parameter to be determined and ${}_2F_1$ is the Gaussian or ordinary hypergeometric function, which arises from the integration of $E(p)$. The alternative formulations for eddy life time, which were provided by Mann[10] and the references within, give different k-proportionalities for the scales larger than the inertial sub-range, such as k^{-2} and $k^{-7/2}$ for $k \to 0$.

The analytical forms of $\Phi_{ij}(\boldsymbol{k})$ in M94 can be expressed as

$$\Phi_{ij}(\boldsymbol{k}) \equiv \Phi_{ij}(\boldsymbol{k}, \alpha\epsilon^{2/3}, L, \Gamma), \tag{7}$$

where time t was substituted by $\tau(k)$. Equation (7) can also be given as

$$\Phi_{ij}(\boldsymbol{k}, \alpha\epsilon^{2/3}, L, \Gamma) = \alpha\epsilon^{2/3} L^{11/3} \Phi_{ij}(\boldsymbol{k}L, 1, 1, \Gamma) \tag{8}$$

and $\Phi_{ij}(\boldsymbol{k}_0) = \alpha\epsilon^{2/3} L^{11/3} \Phi_{ij}(\boldsymbol{k}L, 1, 1, 0)$. So the model contains three adjustable parameters that were determined from the single-point measurements. These three parameters were as follows:

- $\alpha\epsilon^{2/3}$ from equation (5)
- L, which represents the size of the energy containing eddies
- Γ, from equation (6), which is a measure of turbulence anisotropy

Using equation (7), the cross-spectrum between any two velocity components can be given as

$$\chi_{ij}(k_1, \alpha\epsilon^{2/3}, L, \Gamma, \Delta y, \Delta z) = \int \Phi_{ij}(\boldsymbol{k}, \alpha\epsilon^{2/3}, L, \Gamma) \exp\left[\mathrm{i}(k_2\Delta y + k_3\Delta z)\right] \mathrm{d}\boldsymbol{k}_\perp, \tag{9}$$

where $\int \mathrm{d}\boldsymbol{k}_\perp = \int_{-\infty}^{\infty}\int_{-\infty}^{\infty} \mathrm{d}k_2 \mathrm{d}k_3$. Δy and Δz are transverse and vertical separations, respectively. Using equation (9), the single-point power spectrum of the ith velocity component (where $\Delta y = \Delta z = 0$) can be given as $F_i(k_1, \alpha\epsilon^{2/3}, L, \Gamma) = \chi_{ii}(k_1, \alpha\epsilon^{2/3}, L, \Gamma, 0, 0)$ (with no index summation).

The three parameters at any height z were calculated by fitting model $\chi_{ij}(k_1, \alpha\epsilon^{2/3}, L, \Gamma, 0, 0)$ with measured power spectra (including co-spectrum of u ($i = 1$) and w ($j = 3$)) from equation (1) and using Taylor's hypothesis: $k_1 = 2\pi f/U$, where U is the mean wind speed at z. For vertical separations Δz, coherences and cross-spectral phases were defined, respectively, as

$$\mathrm{coh}_{ij}(\overline{k_1}, \overline{L}, \overline{\Gamma}, \Delta z) = \frac{|\chi_{ij}(\overline{k_1}, \alpha\epsilon^{2/3}, \overline{L}, \overline{\Gamma}, \Delta z))|^2}{F_i(\overline{k_1}, \alpha\epsilon^{2/3}, \overline{L}, \overline{\Gamma}) F_j(\overline{k_1}, \alpha\epsilon^{2/3}, \overline{L}, \overline{\Gamma})}, \tag{10}$$

$$\varphi_{ij}(\overline{k_1}, \overline{L}, \overline{\Gamma}, \Delta z) = \arg(\chi_{ij}(\overline{k_1}, \alpha\epsilon^{2/3}, \overline{L}, \overline{\Gamma}, \Delta z)), \tag{11}$$

where $\overline{L}$ and $\overline{\Gamma}$ are the average of L and Γ parameters at two heights z_1 and z_2 (so that $\Delta z = z_2 - z_1$), and $\overline{k_1} = 4\pi f/(U_1 + U_2)$. The model coherences and cross-spectral phases are independent of $\alpha\epsilon^{2/3}$, which can be seen from equation (8) and the definitions described earlier.

The M94 model assumes zero Coriolis force and a uniform shear $\mathrm{d}U/\mathrm{d}z$, which is constant with height. We do not expect that the curvature of the atmospheric boundary layer (ABL) velocity profile (i.e., non-zero $\mathrm{d}^2U/\mathrm{d}z^2$) would alter the results significantly; however, because the three parameters were determined from the single-point measurements, one should expect these parameters to vary with height.

Let us consider the performance of the three parameters with respect to the variances and co-variances. A change in $\alpha\epsilon^{2/3}$ causes a shift of the spectra in the ordinate direction; an increase in $\alpha\epsilon^{2/3}$ results in shifting of u, v and w spectra up and uw co-spectrum down and vice-versa. An increase in L results in shifting of the spectra both to the left along the abscissa and upward along the ordinate and vice-versa. The model assumes initial isotropic turbulence where $\Gamma = 0$, leading to $\sigma_u^2 = \sigma_v^2 = \sigma_w^2$ and $\langle uw \rangle = 0$. For $\Gamma > 0$, the turbulence is anisotropic, i.e., $\sigma_u^2 > \sigma_v^2 > \sigma_w^2$ and $\langle uw \rangle < 0$, so Γ describes the anisotropic nature of turbulence. The various length scales of the velocity components can be calculated as functions of L and Γ. Higher values of Γ imply larger scale separation between the three velocity components, and the length scale of u is greater than that of v, which again is greater than that of w.

3. ANALYSIS AND RESULTS

We showed the velocity spectra and uw co-spectrum from Ryningsnäs and Høvsøre met masts measured at 80 m height for NNS, N and NNU stratifications along with the model fits. The cross-spectra between 80–100 m height were then analyzed using the average of the three parameters determined at these two heights as an input.

3.1. Spectra

The measured velocity spectra along with the model spectral fits for NNS, N and NNU are shown in Figures 2, 3, and 4, respectively, for Ryningsnäs (left graphs) and Høvsøre (right graphs) sites. The power spectral densities at the Ryningsnäs site were observed to be higher than those of the Høvsøre site, because of the higher roughness. The mesoscale motions,
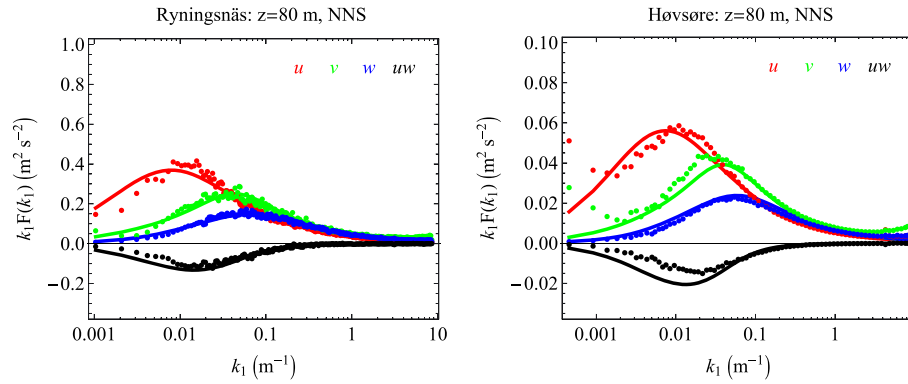

Figure 2. M94 model spectral fits to the observations at Ryningsnäs (left graph) and Høvsøre (right graph) sites for the velocity bin 7–8 ms^{-1}, for NNS stability. Observed spectra are shown by dots, and the model spectra by solid lines. The number of 30-min time series used and the model parameters at $z = 80$ m are given in Table II.

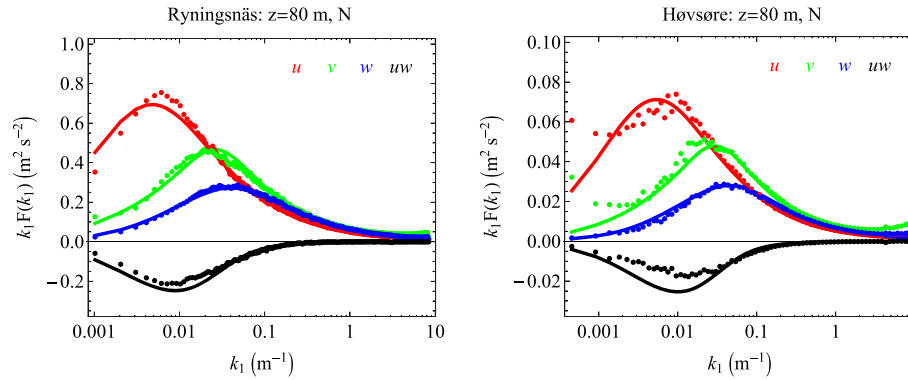**Figure 3.** M94 spectral fits to the Ryningsnäs and Høvsøre measurements in neutral ABLs for the velocity bin 7–8 ms^{-1} at $z = 80$ m. See Figure 2 for the notations.
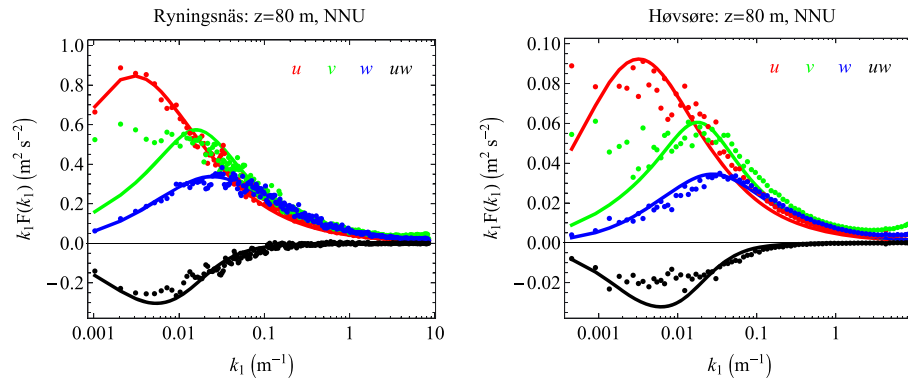

Figure 4. M94 spectral fits to the Ryningsnäs and Høvsøre measurements in NNU ABLs at $z = 80$ m. Notations are the same as before.

identified from the excess power spectral density for $k_1 < 0.002$ m^{-1}, seemed to appear at the Høvsøre site and not at the Ryningsnäs site, which might be because the mesoscale motions at Ryningsnäs were obscured by generally higher turbulence levels at that site. The turbulence level on both sites can quantitatively be seen in terms of variances and co-variances of the velocity components, as given in Table II. Table II also gives an indication of model performance in terms of Δ, which is the model estimation error of the variance relative to the measured variance. A comparison of the Δ values at

Table II. Performance of the model in variance and co-variance predictions in terms of Δ at $z = 80$ m, where Δ is the relative model over/under estimation of the variance.

Stability	$\sigma^2 (m^2 s^{-2})$	Ryningsnäs			Høvsøre		
		Measurements	Model	Δ%	Measurements	Model	Δ%
NNS	σ_u^2	2.92	3.04	+4.35	0.53	0.50	−5.7
	σ_v^2	1.98	1.96	−0.94	0.39	0.31	−20.5
	σ_w^2	1.25	1.26	+0.84	0.18	0.20	+11.1
	$-\langle uw \rangle$	0.67	0.86	+28.72	0.09	0.14	+55.5
N	σ_u^2	5.37	5.34	−0.68	0.66	0.61	−7.6
	σ_v^2	3.68	3.60	−2.11	0.46	0.38	−17.4
	σ_w^2	2.35	2.32	−1.26	0.23	0.24	+4.3
	$-\langle uw \rangle$	1.32	1.54	+17.15	0.12	0.17	+41.7
NNU	σ_u^2	6.11	5.91	−3.24	0.83	0.75	−9.6
	σ_v^2	5.27	4.31	−18.36	0.65	0.48	−26.2
	σ_w^2	2.95	2.83	−3.95	0.30	0.30	0.0
	$-\langle uw \rangle$	1.60	1.75	+9.66	0.17	0.21	+23.5

σ is the standard deviation. The model overestimation is denoted by '+' and underestimation by '−'.

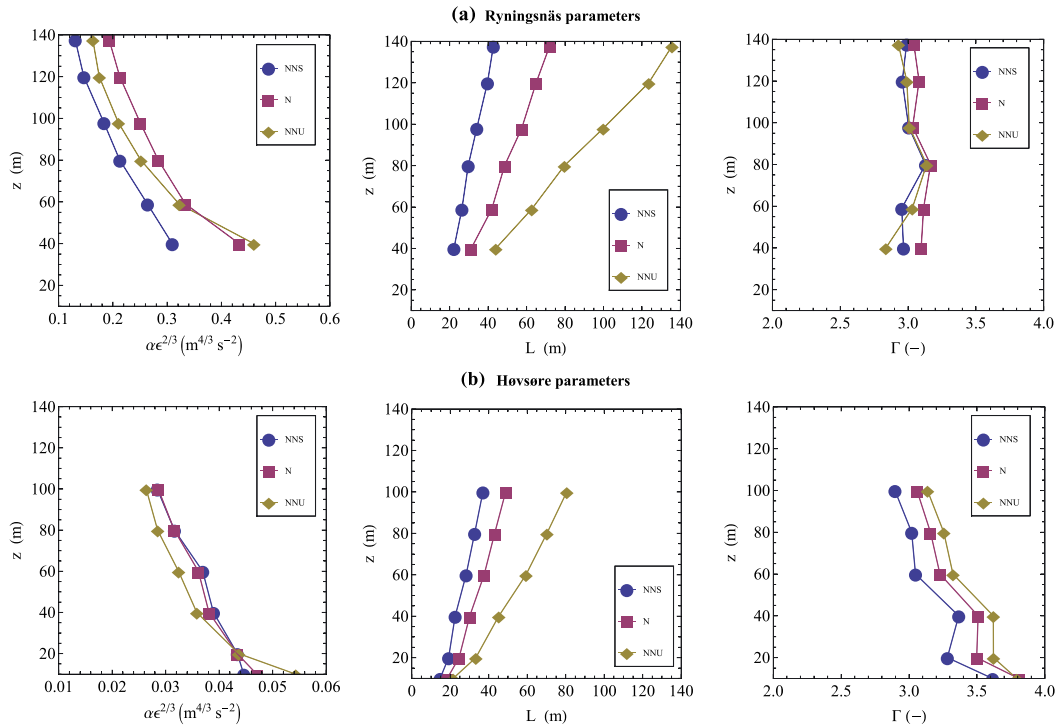**(a)** **Ryningsnäs parameters**

(b) **Høvsøre parameters**

Figure 5. Comparison of the model parameters determined from the single-point measurements for (a) the forested landscapes in Ryningsnäs and (b) the agricultural landscapes in Høvsøre. The three parameters were obtained by performing χ^2-fits.[10] The number of 30-min time series used for each stability case for $z = 80$ m at two sites is given in Table III. Table III also provides the numerical values of the three parameters.

Table III. Three spectral tensor parameters determined from χ^2-fits for NNS, N and NNU stability cases at the Ryningsnäs and Høvsøre sites for the velocity bin 7–8 m s^{-1}.

	Stability	n	$\alpha\epsilon^{2/3}$ (m$^{4/3}$ s^{-2})	L (m)	Γ
			Model parameters		
Ryningsnäs	NNS	60	0.21	29.6	3.13
	N	542	0.28	48.6	3.16
	NNU	33	0.25	79.7	3.14
Høvsøre	NNS	256	0.032	32.8	3.02
	N	226	0.032	43.2	3.16
	NNU	68	0.028	70.4	3.26

The number of 30-min time series n for each case at a given site is also provided in the table. The measurements are taken from sonic anemometers located at $z = 80$ m.

the Ryningsnäs and Høvsøre sites revealed that the model performs relatively better in Ryningsnäs than Høvsøre, particularly for neutral stability. The Δ value of the *uw* co-variance was quite significant for Høvsøre NNS and N cases, and it decreased at both the sites going from NNS to NNU. The values of TKE in Ryningsnäs were $\sim 5, \sim 8.5$ and ~ 8 times those in Høvsøre, for NNS, N and NNU, respectively.

Comparing the model parameters determined at the given sonic heights from two sites (Figure 5), we found that the three model parameters from Ryningsnäs behaved similarly to those from a flat agricultural terrain. The three model parameters determined at 80 m from the two sites, along with the number of 30-min time series n, are shown in Table III. The value of $\alpha\epsilon^{2/3}$ for Ryningsnäs was 8.75 times that for Høvsøre at $z = 80$ m for the neutral case. There was no significant difference in the L vertical profile beyond $z = 40$ m between the two sites. The length scales from the two sites were similar, with the notable difference that L for the NNU case at Ryningsnäs was 24% higher than that at Høvsøre at $z = 100$ m. The turbulence length scales L for all stabilities were found to increase with height, with L for NNU being the greatest. There was a very slight difference in the turbulence anisotropy at the two sites except at 40 m, where the Ryningsnäs turbulence was as much as $\sim 22\%$ more isotropic (for NNU). The turbulence anisotropy remained more or less constant with height at Ryningsnäs, whereas the turbulence became slightly more isotropic with height at Høvsøre.

3.2. Cross-spectra

The model coherences and cross-spectral phases were calculated using equations (10) and (11), respectively. The coherence comparisons are shown in Figure 6. The values of $\overline{L}, \overline{\Gamma}$ at Ryningsnäs were as follows: for NNS: 32 m, 3; N: 53 m, 3.1; and NNU: 90 m, 3.1; those for Høvsøre were as follows: NNS: 35 m, 2.9; N: 46 m, 3.1; and NNU: 75 m, 3.2. Atmospheric stability was found to affect the coherence that increased from stable to unstable stratification. Thermal stability had the most noticeable effect on the *w*-coherence, while the *u*-coherence was less affected by it. From Figure 6, it can be observed that the *u*-coherence is maximum at lower frequencies ($k_1\Delta z \leq 0.2$ for NNS and 0.1 for NNU) and reduces more quickly with $k_1\Delta z$. The model overestimated *u*-coherence, *v*-coherence and *w*-coherence at both the sites for all the given ABLs.

In order to assess the performance of the model in coherence predictions, we defined a factor G, such that

$$G = \int_0^3 |\text{coh}_n(k_1\Delta z) - \langle\text{coh}_{n,t}(k_1\Delta z)\rangle| \text{d}(k_1\Delta z), \qquad (12)$$

which is the absolute area between the coherence estimated from n segments of the time series $\text{coh}_n(k_1\Delta z)$ (dashed lines in Figure 6) and the theoretically predicted coherence $\langle\text{coh}_{n,t}(k_1\Delta z)\rangle$ (smooth lines). The model performance in terms of G at both sites is given in Table IV for the coherences shown in Figure 6. For a perfect theory, the value of G should be close to zero. The model performed relatively better in predicting the *u*-coherence at both sites for neutral stability and relatively poorly for predicting the *v*-coherence at both sites for all three stabilities.

The cross-spectral phases are shown in Figure 7, where it can be observed that $\varphi_v > \varphi_u > \varphi_w$. For NNS, φ_v and φ_u at Ryningsnäs were observed to be greater than those at Høvsøre. The phase shift increases with $k_1\Delta z$ ($0 < k_1\Delta z < 1$) as long as the coherence is non-zero. From Figure 7, it is observed that the cross-spectral phases decreased slightly from NNS to NNU. The phase results from the forested area were consistent with those of the study by Chougule *et al.*[21]
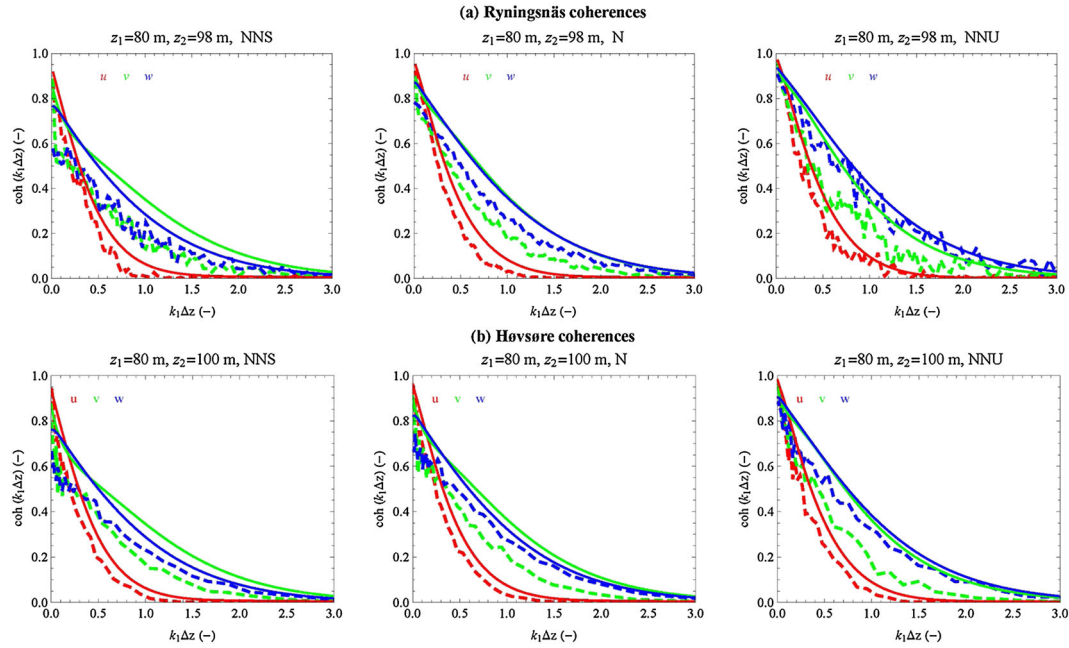
Figure 6. Comparison of the coherences from the measurements (dashed lines) and the model predictions (solid lines) for the two sites: (a) Ryningsnäs and (b) Høvsøre. The average of the three parameters between two given heights was used to determine model cross-spectra using equation (9), and the coherences were calculated from equation (10).

Table IV. Model performance in terms of G factor in coherence predictions according to equation (12).

		G	
Stability	coh	Ryningsnäs	Høvsøre
	u	0.15	0.12
NNS	v	0.37	0.33
	w	0.21	0.16
	u	0.12	0.11
N	v	0.31	0.33
	w	0.17	0.12
	u	0.16	0.15
NNU	v	0.32	0.35
	w	0.16	0.17

The coherences are shown in Figure 6.

4. DISCUSSION

As can be seen from the left graphs of Figures 2–4, the RDT model was able to fit the one-dimensional u-spectra, v-spectra, w-spectra and uw co-spectrum reasonably well for forested flow in neutral and near-neutral ABLs. The Δ values from heights other than 80 m, and the velocity bins other than 7-8 ms^{-1} (5-6 and 6-7 ms^{-1}) were consistent with Table III with Δ for $\langle uw \rangle$ being greatest.

For the Ryningsnäs spectra, we see that the spectra shifted upwards along the ordinate from NNS (via N) to NNU, implying that the turbulent energy increased from NNS to NNU. However, the Ryningsnäs $\alpha \epsilon^{2/3}$ and L curves (top row, first two graphs in Figure 5) show that the $\alpha \epsilon^{2/3}$ values were rather smaller, whereas the L values were greater for NNU case. So the increased turbulence due to buoyancy effects was expressed in increased length scales, which can also be seen from Høvsøre results. Also since the length scales from the two sites were more or less the same, the increased turbulence due to the higher roughness was articulated more as an increased $\alpha \epsilon^{2/3}$. Because u_* at Ryningsnäs was larger (given that
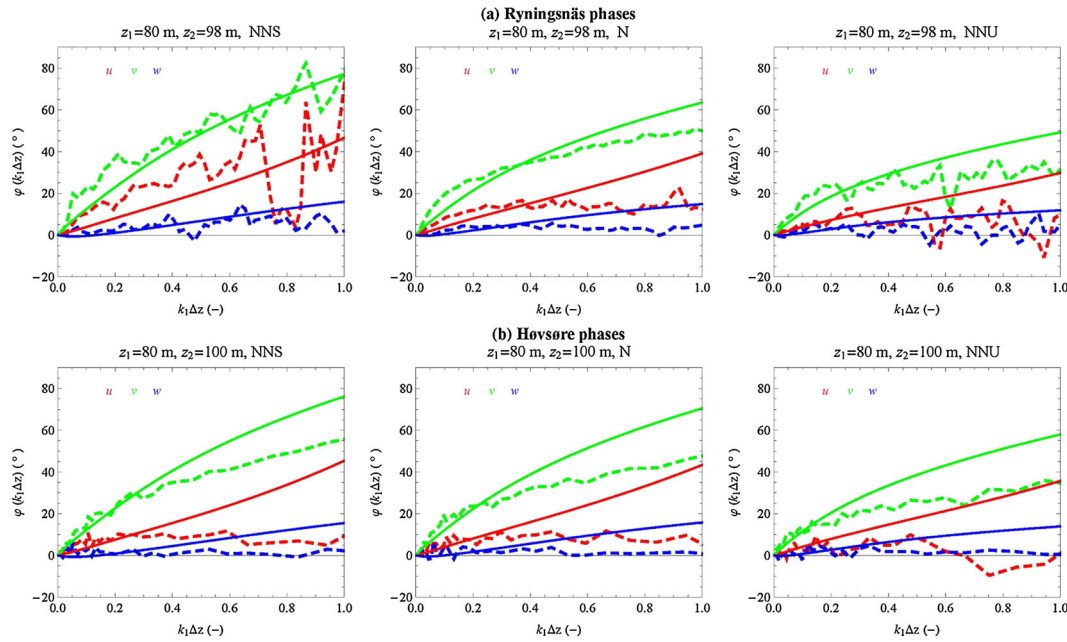
Figure 7. Comparisons of cross-spectral phases between two heights from model predictions and observations for the (a) Ryningsnäs and (b) Høvsøre sites. The model phases were calculated using equation (11).

$\epsilon^{2/3} \propto u_*^2$), for a given L_o, the kinematic heat flux was also larger, resulting in the higher ABL depth. This might have an influence on the length scale, particularly in NNU case, as discussed in Section 3.1.

The three parameters from both the sites varied in similar pattern with height for other wind speed bins for all the three stabilities. For lower wind speed bins, both at the Ryningsnäs and Høvsøre sites, the $\alpha\epsilon^{2/3}$ curves shifted to the left with $\alpha\epsilon^{2/3}$ at Ryningsnäs being approximately 10 times than that at Høvsøre, while L for NNU was slightly decreased, whereas, at Ryningsnäs, Γ remained more or less constant, and the turbulence at Høvsøre became more isotropic with height. From equation (8), it can be observed that the ratio between any two variances (or co-variances) becomes function only of the Γ parameter, so the turbulence anisotropy can directly be represented in terms of that parameter.

For neutral ABLs at Ryningsnäs, there was no significant variation in L or Γ with the mean wind speed bins 4–5, 5–6, 6–7, 7–8, 8–9, 9–10 and 10–11 ms^{-1}. The standard deviations calculated from these seven wind speed bins were ~ 3.0 m and ~ 0.05 at $z = 80$ m, respectively. This was consistent with the results from the Høvsøre site, as discussed by Sathe *et al.*[20] From equations (10) and (11), it can be seen that the model coherences and cross-spectral phases are functions of L and Γ, so they should change very slightly with the mean wind speed in the neutral ABLs, which was also observed from the measurements. With L and Γ at Ryningsnäs insignificantly different from those at Høvsøre, only slight differences of the coherences and the phases between the two sites for NNS, N and NNU were expected (Figures 6 and 7), which was consistent with observations. The earlier discussion was consistent with an other investigated height separation (40–100 m) and the wind speed bins mentioned earlier, where no significant difference was observed in L and Γ with the mean wind speed for NNS, N and NNU.

Table IV provides information on the performance of the model for coherence predictions for vertical separation. The model performance was better in predicting the u-coherence and w-coherence than v-coherence, whereas the neutral stability predictions were slightly better than NNS and NNU, at both the sites. The model performed almost equally well at both the sites. We considered non-stationary data in order to obtain more realizations. The non-stationarity effects for Ryningsnäs were negligible, except in NNU case where there was a slight increase in σ_u and Γ, and G was reduced by 30%. Analyses of other height intervals showed similar order of G values for all three stabilities for 7–8 ms^{-1}, with G for v-coherence being the greatest ($\gtrsim 0.3$). This was in contrast to the study of Mann,[10] where the w-coherences were predicted poorest (overestimated) by the model. However, in that investigation, the spatial separations were horizontal, not vertical, as in the present investigation. In addition to the different height intervals, the values of G from the other wind speed bins were consistent with Table IV for NNS, N and NNU, which could be because the model coherence is a function of L and Γ, which changed insignificantly with the mean wind speed for the three stabilities.

Because neither L nor Γ differ significantly between the two sites, and from the fact that high turbulence levels in forested areas increased loads on the rotor, we would like to analyze $\alpha\epsilon^{2/3}$ further. Figure 8 shows the neutral asymptotic
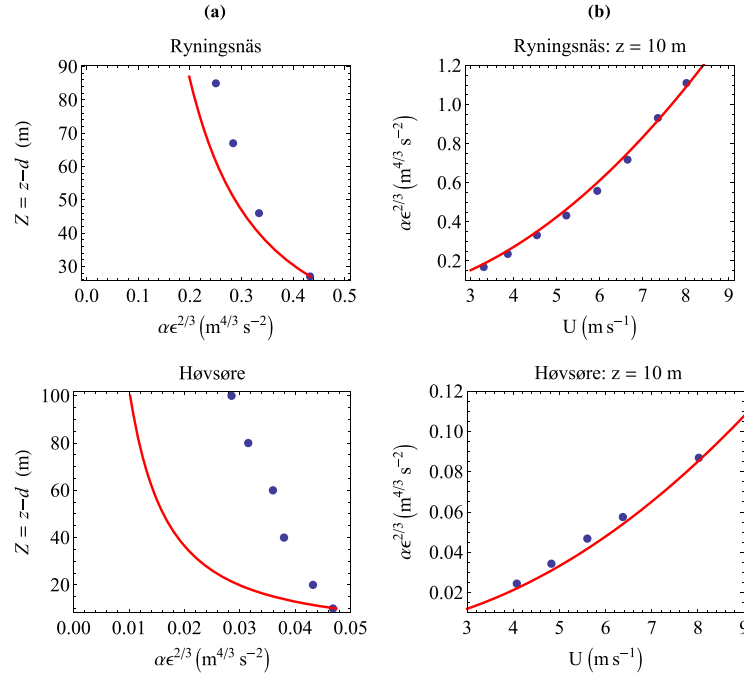
Figure 8. Variation of $\alpha\epsilon^{2/3}$, shown by dots with Z at 7–8 ms^{-1} [column (a)] and U [column (b)], where $Z = z - d$. The displacement height d for Ryningsnäs is 13 m, and that for Høvsøre is 0. The solid lines are the neutral surface-layer scaling: $\alpha\epsilon^{2/3} \propto Z^{-2/3}$ in column (a) and $\alpha\epsilon^{2/3} \propto U^2$ in column (b).

limits:[1] $\epsilon \propto U^3/Z$ with $Z = z - d$ for Ryningsnäs and $Z = z$ for Høvsøre, where $d = 13$ m is the displacement height.[25] It can be observed from the Z vs. $\alpha\epsilon^{2/3}$ curve that, at Høvsøre, the dissipation rate decreased with height more slowly than expected, which might be because the site was not completely homogeneous toward the east. It is known that rough-to-smooth transitions can be felt extremely far downstream from the transition location.[28] The lowest points on the Z vs. $\alpha\epsilon^{2/3}$ curve are influenced by the relatively smooth terrain close to the site, while the points further up have larger ϵ than expected because of the trees and forest further east. The dots in the right graphs of the Figure 8 correspond to the velocity bins measured at $z = 80$ m, where for Ryningsnäs, we selected eight velocity bins from 4–5 to 11–12 m s^{-1}, while for Høvsøre, the velocity bins were 5–6, 6–7, 7–8, 8–9 and 10–11 m s^{-1}.

Because of the limited number of realizations n, there is uncertainty in the estimated (cross-) spectra and hence in the corresponding coherences and phases. Kristensen and Kirkegaard[2] showed that the coherence was systematically overestimated. However, the overestimation was insignificant for the n values in Table II. The variance of the phase estimate for u, v and w from Kristensen and Kirkegaard[2] increased with $k_1\Delta z$, with the largest value of the standard deviation being 26° and 19° in φ_u for NNU at $k_1\Delta z \approx 1$ at Ryningsnäs and Høvsøre, respectively.

5. CONCLUSION

Our aim in this study was to investigate the performance of the RDT-based spectral tensor model in predictions of the velocity spectra, co-spectra and cross-spectra over the forested area and to compare the results with those from the agricultural landscapes. The RDT model was found to be able to fit the one-dimensional spectra quite well over the forested area. In terms of variances and co-variances, the model performed relatively better in forested area, particularly for neutral ABLs. The spectral tensor model needs only three parameters to describe the spectra: the viscous dissipation rate of TKE, a length scale and a parameter describing the turbulence anisotropy. The dissipation rate of TKE over the forest canopy was nine times that over smooth agricultural landscapes. No significant difference was observed in the variations of length scales with height between forested and agricultural areas, while the length scales over the forest canopy were more or less similar to those over agricultural landscapes. The turbulence anisotropy remained more or less constant with height over forested area, whereas it decreased slightly with height in agricultural landscapes. No significant difference was observed in the turbulence anisotropy of the two sites.

The coherences from the RDT model were independent of the dissipation rate of TKE, which was also supported by the measurements. Despite good spectral fits, the model overestimated coherence of all the three velocity components for vertical separations. It performed relatively better in predicting the *u*-coherence in all stabilities; however, its *v*-coherence prediction was relatively poor at both the sites. The model performed slightly better for neutral stability than for slightly stable and unstable stratification at both the sites. Generally, there was no large difference between the performance of the model in predictions at the forested and agricultural areas. The flow over forest showed similar phase shifts to those over the agricultural areas. Finally, the dissipation rate parameter of the model was evaluated against a standard expression for neutral surface-layer scaling, where the agreement was better at Ryningsnäs than at Høvsøre.

ACKNOWLEDGEMENTS

REFERENCES

1. Kaimal JC. Finnigan JJ. *Atmospheric Boundary Layer Flows*. Oxford University Press: New York, 1994.
2. Kristensen L, Kirkegaard P. Sampling problems with spectral coherence. *Risø report Risø-R-526* February 1986.
3. Townsend AA. *The Structure of Turbulent Shear Flow* (2nd edn). Cambridge University Press: UK, 1976.
4. Tennekes H, Lumley JL. *A First Course in Turbulence*. MIT Press: Cambridge, 1972.
5. Davenport AG. The spectrum of horizontal gustiness near the ground in high winds. *Quarterly Journal of the Royal Meteorological Society* 1961; **87**: 194–211.
6. Tong C, Wyngaard JC. Two-point coherence in the atmospheric surface layer. *Boundary-Layer Meteorology* 1996; **81**: 105–121.
7. Kristensen L, Lenschow DH, Kirkegaard P, Courtney M. The spectral velocity tensor for homogeneous boundary-layer turbulence. *Boundary-Layer Meteorology* 1989; **47**: 149–193.
8. Kaimal JC, Wyngaard JC, Izumi Y, Coté OR. Spectral characteristics of surface-layer turbulence. *Quarterly Journal of the Royal Meteorological Society* 1972; **98**(417): 563–589, DOI: 10.1002/qj.49709841707.
9. Veers PS. Three-dimensional wind simulation. *Technical Report SAND88-0152*, Sandia National Laboratories, March 1988.
10. Mann J. The spatial structure of neutral atmospheric surface-layer turbulence. *Journal of Fluid Mechanics* 1994; **273**: 141–168.
11. Pope SB. *Turbulent Flows* (1st edn). Cambridge University Press: UK, 2000.
12. Maxey MR. Distortion of turbulence in flows with parallel streamlines. *Journal of Fluid Mechanics* 1982; **124**: 261–282.
13. Hanazaki H, Hunt JCR. Linear processes in unsteady stably stratified turbulence. *Journal of Fluid Mechanics* 1996; **318**: 303–337.
14. Hanazaki H, Hunt JCR. Structure of unsteady stably stratified turbulence with mean shear. *Journal of Fluid Mechanics* 2004; **507**: 1–42.
15. IEC. Wind turbines part 1: design requirements. *Techincal Report IEC 61400-1* 2005.
16. Mann J. Wind field simulation. *Probabilistic Engineering Mechanics* 1998; **13**(4): 269–282.
17. Mann J. Models in micrometeorology, *Ph.D. Thesis Risø Rep. R-727(EN)*, University of Aalborg 1994.
18. Peña A, Gryning SE, Mann J. On the length-scale of the wind profile. *Quarterly Journal of the Royal Meteorological Society* October 2010; **136**: 2119–2131.
19. Peña A, Gryning S, Mann J, Hasager CB. Length scales of the neutral wind profile over homogeneous terrain. *Journal of Applied Meteorology and Climatology* 2010; **49**: 792–806.

20. Sathe A, Mann J, Barlas T, Bierbooms WAAM, van Bussel GJW. Influence of atmospheric stability on wind turbine loads. *Wind Energy* 2012, DOI: dx.doi.org/10.1002/we.1528.

21. Chougule A, Mann J, Kelly M, Sun J, Lenschow DH, Patton EG. Vertical cross-spectral phases in neutral atmospheric flow. *Journal of Turbulence* 2012; **13**(36): 1–13, DOI: 10.1080/14685248.2012.711524.

22. Gryning S, Batchvarova E, Brümmer B, Jørgensen H, Larsen S. On the extension of the wind profile over homogeneous terrain beyond the surface boundary layer. *Boundary-Layer Meteorology* 2007; **124**: 251–268.

23. Bechmann A, Berg J, Courtney MS, Jørgensen HE, Mann J, Sørensen NN. The bolund experiment: overview and background. *Risø report Risø-R-1658(EN)*, July 2009.

24. Liu H, Peters G, Foken T. New equations for sonic temperature variance and buoyancy heat flux with an omnidirectional sonic anemometer. *Boundary-Layer Meteorology* 2001; **100**: 459–468.

25. Bergström H, Alfredsson H, Arnqvist J. Carlén I, Dellwik E, Fransson J, Ganander H, Mohr M, Segalini A, Söderberg S, Wind power in forests: winds and effects on loads. *Report*, March 2013. http://www.elforsk.se/Rapporter.

26. Sathe A, Mann J, Gottschall J, Courtney MS. Can wind lidars measure turbulence? *Journal of Atmospheric and Oceanic Technology* 2011; **28**(7): 853–868.

27. von Kármán T. Progress in the statistical theory of turbulence. *Proceedings of the National Academy of Sciences* 1948; **34**: 530–539.

28. Antonia R, Luxton R. The response of a turbulent boundary layer to a step change in surface roughness. Part 2. Rough-to-smooth. *Journal of Fluid Mechanics* 1972; **53**(4): 737–757.